Available online at www.sciencedirect.com

ScienceDirect

Ceramics International 40 (2014) 3785–3791

CERAMICS INTERNATIONAL

www.elsevier.com/locate/ceramint

Deposition of Al_2O_3 by resistive evaporation and thermal oxidation of Al to be applied as a transparent FET insulating layer

Miguel Henrique Boratto, Luis Vicente de Andrade Scalvi*

Physics Department, POSMAT – FC, UNESP São Paulo State University, Bauru, SP, Brazil

Received 31 July 2013; received in revised form 10 September 2013; accepted 11 September 2013
Available online 18 September 2013

Abstract

Alumina thin films have been obtained by resistive evaporation of Al layer, followed by thermal oxidation by means of annealing in appropriate atmosphere (air or O_2-rich), with variation of annealing time and temperature. Optical and structural properties of the investigated films reveal that the temperature of 550 °C is responsible for reasonable oxidation, which is accelerated up to 8 times for O_2-rich atmosphere. Results of surface electrical resistivity and Raman spectroscopy are in good agreement with these findings. Surprisingly, X-ray and Raman data suggest also the crystallization of Si nuclei at glass substrate–alumina interface, which would come from the soda-lime glass used as substrate.

Keywords: Alumina; Resistive evaporation; Thermal annealing; Oxidation

1. Introduction

Alternative insulating materials with desired properties enabling the use in field effect transistors (FET) have been of great interest in the past recent years, mainly for substitution of silicon dioxide (SiO_2) in the role of gate layer [1–7]. Aluminum oxide (Al_2O_3), also known as alumina, is an insulator material widely used as dielectric gate, tunneling barrier and protection coating [1,8]. It has been distinguished as an insulating material presenting several interesting properties such as high dielectric constant (high-*k*), large bandgap, high adherence to several sort of materials and good thermal and mechanical stability [1,3–9], being suitable to be used as dielectric gate, where it shows low leakage current and low density of interface defects. Materials with high-*k* used as gate dielectrics lead to larger capacitance layers, which becomes more efficient as the dielectric constant gets higher. For instance, when comparing layers with the same thickness for the dielectric gate role, the high-*k* material presents higher capacitance as well as higher current through the conduction channel. Moreover, the lower tunneling probability of a high-*k* material gate reduces the leakage current [4].

The electron transport in the high-*k* Al_2O_3 is mainly due to oxygen vacancies and intrinsic defects originated from oxygen deficiency. At high temperatures, the electron transport is consistent with Poole–Frenkel conduction, due to field-enhanced thermal excitation of trapped electrons from an intra-bandgap trap state located 1.5–1.8 eV below the conduction band bottom [5,8].

All of these relevant properties contribute to Al_2O_3 be proposed for use in the gate of metal oxide field effect transistor (MOSFET), turning out to be competitive to the system SiO_2/Si, in substitution to the traditional silicon dioxide gate layer. Al_2O_3 allows the modulation of the electronic transfer between source and drain with higher efficiency. This is the case of the system Al_2O_3/GaAs presented by Lin and coworkers [8], which shows a leakage current one order of magnitude lower than the system SiO_2/Si [1,8].

Besides the use of Al_2O_3 as gate dielectrics in MOSFET [1], it may be also utilized in metal oxide semiconductor (MOS) capacitors [5], in thin film transistor (TFT) [6], in transparent and flexible TFT [7] and graphene-based FET [3]. These applications were obtained using several types of deposition of Al_2O_3.

In this work, aluminum oxide films are obtained from metallic aluminum deposition on glass substrates, followed

*Corresponding author. Tel.: +55 14 31036084.
E-mail addresses: scalvi@fc.unesp.br, luis.scalvi@pq.cnpq.br (L.V. de Andrade Scalvi).

0272-8842/$ - see front matter © 2013 Elsevier Ltd and Techna Group S.r.l. All rights reserved.
http://dx.doi.org/10.1016/j.ceramint.2013.09.041

by thermal annealing, which induces oxidation to alumina. Thermal annealing conditions, such as temperature and time are varied [10,11], and the optical and structural properties are investigated by X-ray diffraction (XRD), UV–vis transmittance spectra, Fourier transform infrared (FTIR) spectroscopy, and Raman spectroscopy. Surface resistivity is also measured in order to help the understanding of thermal oxidation process. The metallic films are deposited by resistive evaporation technique and the thermal annealing is carried out under different O_2-concentration atmospheres, allowing the oxygen diffusion and surface crystalline structure modification [12].

2. Experimental

The deposition of aluminum oxide thin films consists basically of two steps: (1) resistive evaporation of metallic aluminum layer on soda-lime glass substrate and (2) thermal annealing (TA) of the deposited film. The precursor metallic aluminum, in the form of powder, was placed in tungsten crucible, inside a Boc Edwards Auto 500 evaporation system under low pressure (about 10^{-5} mbar). During the evaporation process the substrates were kept under rotation attached to the sample holder, in order to get a better homogeneity [13]. A crystalline quartz sensor was located inside the evaporation chamber, being responsible for evaluation of the film thickness. The evaporation rate was in the range 0.3–0.6 nm s^{-1} until reaching a final thickness of about 140 nm.

TA of the aluminum films is carried out at different temperatures: 400, 500 and 550 °C, in atmospheric (air) or O_2-rich conditions, for time varying from 2–24 h. The maximum TA temperature was chosen as 550 °C due to limitations concerning the aluminum melting temperature (about 660 °C) [12] and mainly due to the vitreous transition of the soda-lime glass substrate (about 560 °C) [14]. Then, a temperature above 550 °C could cause softening of the glass, leading to film loss of adherence. Samples were treated in atmosphere conditions in an EDG 3P-S 1800 oven, whereas for samples treated in O_2-rich conditions, it was used an EDGCON 5P oven equipped with a quartz tube. In this last case, the pressure was lowered down to 10^{-5} mbar and then the oven was filled with O_2 until 1 atm. Table 1 lists the TA used for all the samples, concerning temperature, time and O_2-concentration conditions. In order to get a reasonable comparison among samples, they were divided in two types: (1) samples submitted to multiple TA (M1A–M5A) and (2) samples submitted to a sole TA (S1A–S6O), where "A" and "O" in the code of samples refer to the atmosphere (air or O_2, respectively) of the TA.

XRD measurements were done in a Rigaku D/Max-2100PC diffractometer, coupled with a CuKα (0.15406 nm) radiation source and Ni filter for elimination of CuKβ line. All data were treated with the program Peak Search. UV–vis transmittance was done in Perkin Elmer equipment, model Lambda 1050. FTIR was carried out in the ATR mode in the range 350–4000 cm^{-1} in a Bruker equipment, model Vertex 70. Raman spectra were obtained with excitation by the 488 nm line of an Ar^+ laser from Spectra-Physics, model Stabilite 2017 focused to 50× magnification, with laser spot of diameter 5 μm irradiated on the sample surface. The Raman signal was collected with a triple monochromator Jobin Yvon model T64000 in backscattering configuration. Electrical resistivity evaluation was done by measuring the surface resistance with a Keithley electrometer, model 617, and using the sample dimensions (Ohms's second Law).

3. Results and discussion

Fig. 1 shows X-ray diffractograms (Fig. 1a) and UV–vis transmittance (Fig. 1b) of samples submitted to several TA. It can be seen that samples M1A, M2A and M4A even after several TA in air, still show the crystalline structure of face-centered cubic (FCC) aluminum, with very intense peaks at 38.4°, 44.5°, 65.3° and 78.2° corresponding to planes with Miller's indexes (111), (200), (220) and (311) respectively, according to the file JCPDS-ICDD 2003 no. 89-2769. Besides, it shows a slight oxidation, as can be noticed by the showing up of low intensity peaks at 37.7°, 39.5°, 45.8° and 66.8°,

Table 1
Thermal annealing conditions for all the aluminum deposited films.

Sample	1st TA	2nd TA	3rd TA
M1A	400 °C 2 h air	500 °C 2 h air	550 °C 4 h air
M2A			550 °C 8 h air
M3AO			550 °C 4 h O_2

	1st TA	2nd TA	3rd TA	4th TA	5th TA
M4A	500 °C 4 h air	500 °C 6 h air	500 °C 8 h air	500 °C 10 h air	500 °C 16 h air
M5A	550 °C 4 h air	550 °C 6 h air	550 °C 8 h air	550 °C 10 h air	550 °C 16 h air

	Sole TA
S1A	550 °C 16 h air
S2A	550 °C 20 h air
S3A	550 °C 24 h air
S4O	500 °C 4 h O_2
S5O	550 °C 2 h O_2
S6O	550 °C 6 h O_2

related to the planes (311), (222), (400) and (440), of the FCC aluminum oxide, file JCPDS-ICDD 2003 no. 77-0396. Samples M3AO and M5A, thermally annealed at 550 C, show higher oxidation level after TA of 4 h in O_2-rich atmosphere and 16 h in air, respectively. The respective XRD pattern presents low intensity peaks at 65.3° and 78.2° related to FCC Al, and the appearing of the peaks at 37.7°, 39.5° 45.8°, 60.9° and 66.8° related to the planes (311), (222), (400), (333) and (440), respectively, of the FCC alumina. Surprisingly, the XRD pattern shows peaks at 28.4°, 47.3° and 56.2°, which are probably related to FCC crystalline silicon, associated to planes (111), (220) and (311), respectively, of the file JCPDS-ICDD 2003 no. 27-1402. This silicon could be originated from the crystallization of the component Si of the soda-lime glass substrate, taking place at the interface with the oxidized Al film [18]. It would be in good agreement with induced Si crystallization by metallic Al [15–19], obtained by AIC technique (aluminum-induced crystallization), where the silicon nucleates on the Al surface. It is well known that amorphous Si in contact with certain metals crystallizes well below the eutectic temperature of the aluminum/silicon system [15].

UV–vis transmittance of these samples (Fig. 1b) illustrates the difference between aluminum films with very low oxidation (M1A, M2A and M4A) and films with higher oxidation level to alumina (M3AO and M5A). In the first case, films are rather opaque in the investigated range (200–1000 nm) whereas oxidized films are partially transparent at beginning of the analyzed wavelength range and have increasing transparency in the visible range.

All samples revealed with alumina structure, correspond to FCC aluminum oxide (JCPDS-ICDD 2003 no. 77-0396), whereas the peaks of aluminum correspond to FCC Al (JCPDS-ICDD 2003 no. 89-2769) and the structure of silicon corresponds to FCC Si (JCPDS-ICDD 2003 no. 27-1402). All the XRD experimental data are compared to the respective crystallographic file as listed in Table 2.

Fig. 2 shows XRD and UV–vis transmittance data for samples submitted to a sole TA for long times. Films with a sole TA in O_2-rich atmosphere (S4O, S5O and S6O) or in air (S1A, S2A and S3A), with annealing time superior to 2 and 16 h, respectively, show fair oxidation only for TA temperature of 550 °C. This is evidenced in Fig. 2. These films present a complete modification on the XRD pattern from aluminum to alumina, with the only exception of film S4O, which shows low oxidation level even in O_2-rich atmosphere, probably due to TA temperature of 500 °C. The diffractogram corresponding to this film evidences only two alumina peak, at 45.8° and 66.8°, and a maximum transmittance of about 15%, whereas the transmittance for the other samples are much higher, mainly for the visible range, as can be seen in Fig. 2b. The peaks found in the XRD data of samples shown in Fig. 2 are listed in Table 3.

The average crystallite size, evaluated through the Scherrer equation [20] for films with Al_2O_3 crystalline structure, was

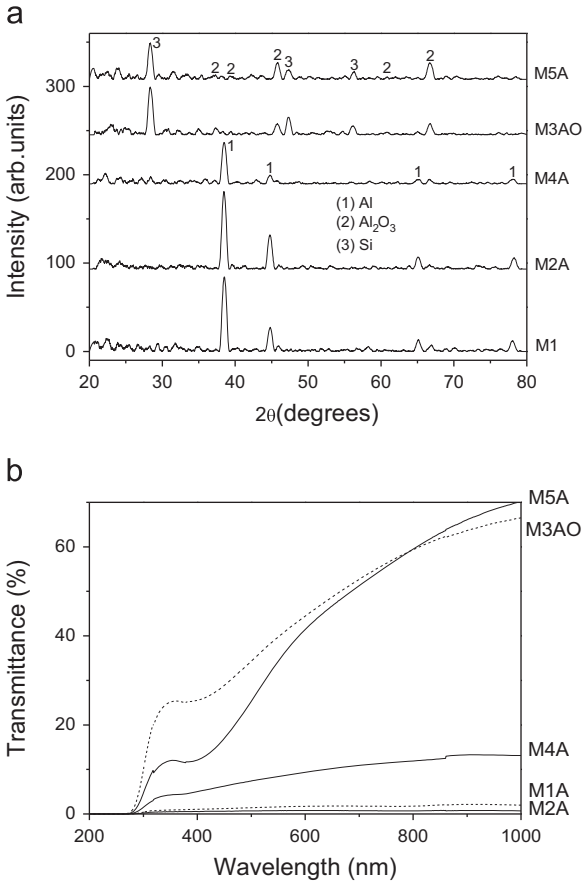

Fig. 1. (a) XRD and (b) UV–vis transmittance of films submitted to several TA.

Table 2
Comparison between experimental diffraction data and the literature for films submitted to several TA, and related planes with respective Miller's index (*hkl*).

Samples	Experimental	FCC Al[a]	FCC Al_2O_3[b]	(*hkl*)
M3AO, M4A, M5A	37.7	–	37.7	311
M1A, M2A, M4A	38.4	38.47	–	111
M2A, M3AO, M4A	39.5	–	39.45	222
M1A, M2A, M4A	44.5	44.72	–	200
M1A, M2A, M3AO, M4A, M5A	45.8	–	45.87	400
M3AO, M5A	60.9	–	60.83	333
M1A, M2A, M3AO, M4A, M5A	65.3	65.1	–	220
M1A, M2A, M3AO, M4A, M5A	66.8	–	66.9	440
M1A, M2A, M4A, M5A	78.2	78.23	–	311

[a]File JCPDS-ICDD 2003 no. 89-2769.
[b]File JCPDS-ICDD 2003 no. 77-0396.

about 12 nm. Besides, there is no noticeable difference on the crystallite size concerning the total TA time or atmosphere.

As already mentioned, it seems that the Al oxidation to Al_2O_3 on the film surface takes place simultaneously with a Si layer growth at substrate/Al interface. In this case the Si from the glass substrate diffuses to the interface and crystallizes there [18]. The final assembly of films looks like Fig. 3.

Fig. 4 shows estimation of film resistivity measured at room temperature, concerning total TA time, atmosphere and number of TA. Results are in good agreement with XRD results as well as transmittance spectra. When oxidized, films have the resistivity largely increased, varying up to 6 orders of magnitude, when compared to the metallic Al layers, because Al_2O_3 is a well-known electrical insulator. The temperature

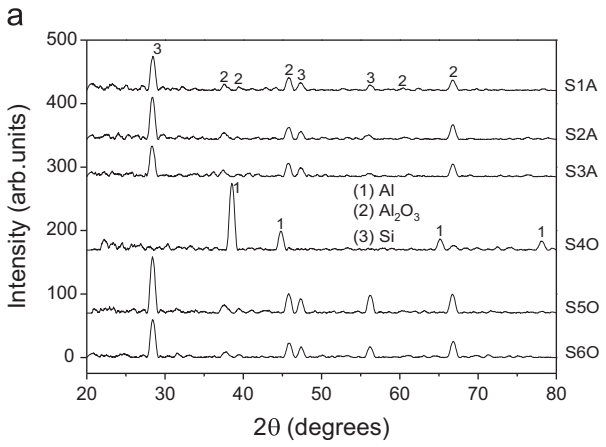

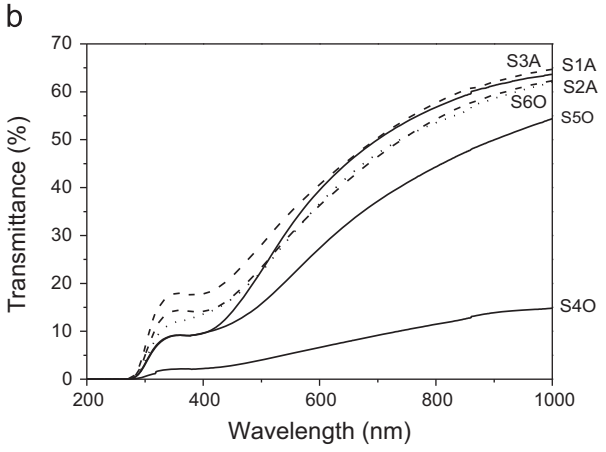

Fig. 2. (a) XRD and (b) UV–vis transmittance of films submitted to a sole TA.

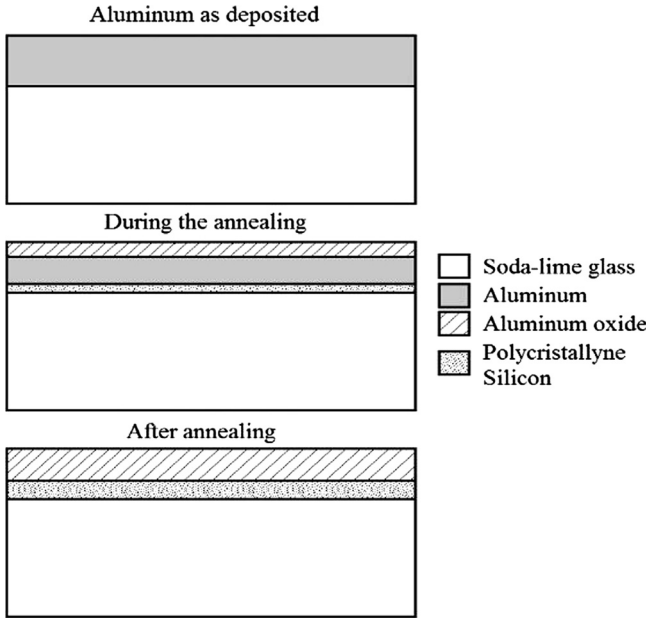

Fig. 3. Schematic diagram of (top) the aluminum film as deposited, (center) during the TA and (bottom) the Al_2O_3 and silicon films after TA.

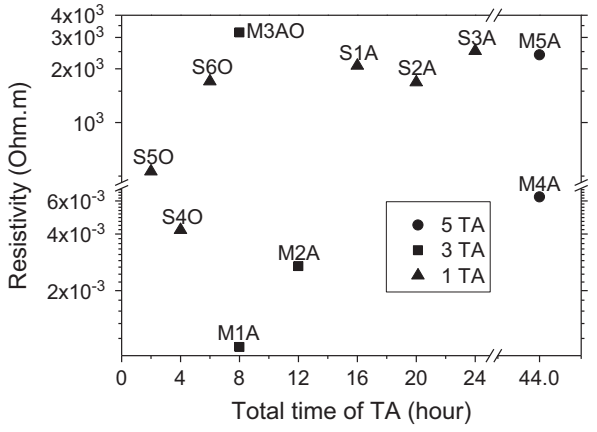

Fig. 4. Film resistivity as function of total TA time and number of TA.

Table 3
Comparison between experimental diffraction data and the literature for films with a sole TA, and respective planes.

Samples	Experimental	FCC Al[a]	FCC Al_2O_3[b]	(*hkl*)
S1A, S2A, S3A, S5O, S6O	37.7	–	37.7	311
S4O	38.4	38.47	–	111
S1A, S2A, S3A, S5O, S6O	39.5	–	39.45	222
S4O	44.5	44.72	–	200
S1A, S2A, S3A, S4O, S5O, S6O	45.8	–	45.87	400
S1A, S2A, S3A, S5O, S6O	60.9	–	60.83	333
S4O	65.3	65.1	–	220
S1A, S2A, S3A, S4O, S5O, S6O	66.8	–	66.9	440
S4O	78.2	78.23	–	311

[a]File JCPDS-ICDD 2003 no. 89-2769.
[b]File JCPDS-ICDD 2003 no. 77-0396.

shift from 500 to 550 °C seems to be limiting a critical transition region, because this temperature variation is the most relevant parameter for the increase of resistivity. TA at 500 °C, even with 44 h of total time, independent on the atmosphere (air or O_2-rich), does not lead to appreciable structural modification neither transmittance increase, in total accordance with the low resistivity, characteristic of metallic films. On the other hand, TA at 550 °C, above 16 h of total TA time, in air, leads to resistivity of about 2.10^3 Ω m, suggesting a tendency for the material to become an insulating material, in good agreement with X-ray diffractogram, and high optical transmittance. Films with TA carried out in O_2-rich atmosphere show resistivity augment with increasing TA total time at 550 °C. For instance, films S5O and S6O, with annealing time of 2 and 6 h, present resistivity of 0.53×10^3 and 1.7×10^3 Ω m, respectively, whereas films S1A, S2A, S3A and M5A, all with TA in air, show resistivity in the range 2×10^3–3×10^3 Ω m, but with total TA above 16 h.

Fig. 5 shows FTIR spectra of selected alumina films. This result shows absorption bands at wavenumber 400, 670, 711 to 745, 882, 1064, 1600, 2300 and 3400 cm^{-1}, some of them (up to 1064 cm^{-1}) vary slightly from a film to another, being the largest variation for the absorption band detected in the range 711–745 cm^{-1}. A small difference in the transmittance intensity among the films is also observed for the whole investigated range. The weak infrared absorption band detected at 1064 cm^{-1} can be associated with the bending mode of Al–OH bond [21,22] and the symmetric vibration mode of Al–O–H bond, similar to what is found in boehmite (AlO(OH)) [23]. The absorption bands at 670 and 711–745 cm^{-1} are related to the vibration mode of Al–O, where the Al has 4 and 6 coordination [21,22,24–26]. The range 400–1000 cm^{-1}, is generally associated with stretching vibrations of the Al–O bond [22]. The most intense bands, observed in Fig. 5 at 400 and 882 cm^{-1}, are in this range and represent the stretching vibrations of Al–O bond in AlO_6 [22,26]. This analysis shows the presence of tetrahedral and octahedral structures of alumina, but also with slight probability of aluminum hydroxide presence, because after thermal annealing above 400 °C, it is supposed that OH molecules are eliminated [21,23]. Noisy and low intense bands about 1600 and 3400 cm^{-1} are related, respectively, to stretching and bending modes of adsorbed H_2O, and the peak about 2300 cm^{-1} is related to CO_2 [21,23]. Either the H_2O vibrations as well as the CO_2 vibrations are often found in FTIR spectra. Table 4 lists infrared absorption data, related to alumina, and comparison with literature.

The same films analyzed by FTIR were also measured by Raman spectroscopy and the results are plotted in Fig. 6. The most prominent bands have peaks at 416, 433, 507 and 604 cm^{-1}, corresponding to molecule vibration in the α-Al_2O_3 [27–29]. Vibration related to frequencies 507, 433 and 401 cm^{-1} indicate the length variation of the Al–O bond of the isolated molecule of AlO_6 in γ-Al_2O_3 and the band at 604 cm^{-1} may be identified as isolated molecule of AlO_4 and condensed groups of AlO_6. Raman bands peaking at 355, 298 and 284 cm^{-1} are attributed to vibration of groups AlO_4 and AlO_6 also in the γ-Al_2O_3 [26].

The very intense peak at 507 cm^{-1} could come from α- [29] and γ-Al_2O_3 [26], which are stable and metastable forms found for alumina. Results of FTIR and Raman show the presence of

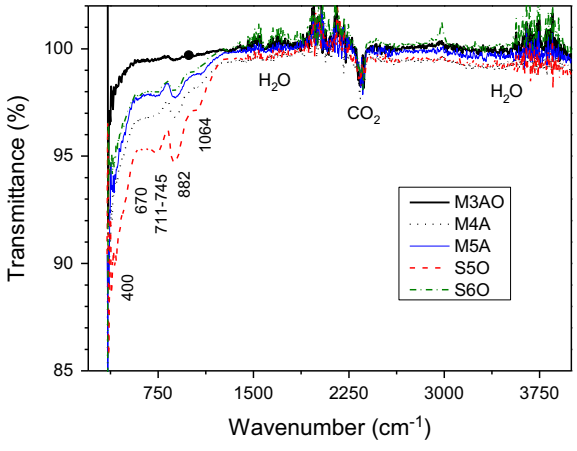

Fig. 5. FTIR spectra of selected alumina films.

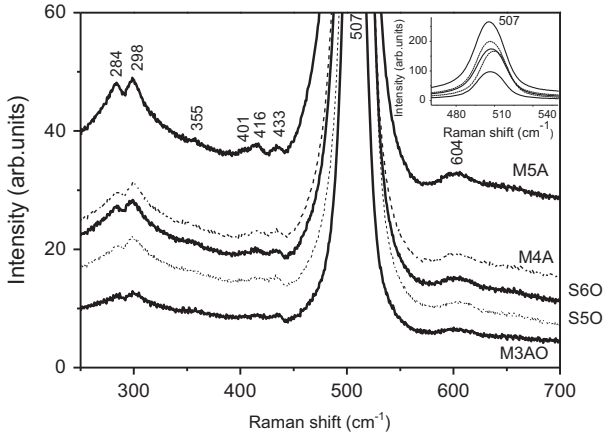

Fig. 6. Raman spectra of the alumina films. Inset: detail of the highest intensity peak.

Table 4
FTIR experimental datas and references.

Experimental	Reference	Reference	Reference	Reference	Material
400 cm^{-1}	414 cm^{-1} [22]	433 cm^{-1} [26]			Al_2O_3
670 cm^{-1}	690 cm^{-1} [21]	635 cm^{-1} [26]			Al_2O_3
711–745 cm^{-1}	737 cm^{-1} [22]	730–760 cm^{-1} [24]	710 cm^{-1} [25]	742 cm^{-1} [26]	Al_2O_3
882 cm^{-1}	898 cm^{-1} [22]	840 cm^{-1} [26]			Al_2O_3
1064 cm^{-1}	1070 cm^{-1} [21]	1065 and 1073 cm^{-1} [23]	1069 cm^{-1} [22]		AlO(OH)

Table 5
Raman experimental data and reference data.

Experimental	Reference	Reference	Reference	Reference	Material
284 cm^{-1}	290 cm^{-1} [26]				γ-Al_2O_3
298 cm^{-1}	315 cm^{-1} [26]				γ-Al_2O_3
355 cm^{-1}	359 cm^{-1} [26]				γ-Al_2O_3
401 cm^{-1}	400 cm^{-1} [26]				γ-Al_2O_3
416 cm^{-1}	418 cm^{-1} [27]	420 cm^{-1} [28]	419 and 418 cm^{-1} [29]		α-Al_2O_3
433 cm^{-1}	445 cm^{-1} [26]	432 cm^{-1} [29]			α-Al_2O_3; γ-Al_2O_3
507 cm^{-1}	519 cm^{-1} [17]	500 and 500–510 cm^{-1} [19]	502 cm^{-1} [26]	492 cm^{-1} [29]	α-Al_2O_3; γ-Al_2O_3; Si
604 cm^{-1}	619, 597 and 610 cm^{-1} [26]	600 cm^{-1} [29]			α-Al_2O_3; γ-Al_2O_3

aluminum oxide in those two structures, agreeing partially with the structure found by XRD, where only a metastable alumina phase was found. The peak at 507 cm^{-1} may also be associated to silicon, which is attributed to nanocrystalline silicon or defective crystalline silicon in Si lattice [19], also referred as polycrystalline Si [17,30]. In this case, the Si would come from the growth at substrate/Al interface [18], as already discussed, in good agreement with some peaks found out the DRX diffractograms. Table 5 lists the experimental Raman bands positions and the possible identification with literature.

Raman data show the possible presence of α-Al_2O_3 in the oxidized material, but the most probable result is the presence of γ-Al_2O_3, which would be in good agreement with the XRD diffraction results. FTIR and Raman of film M4O, which shows metallic Al form, with a slight oxidation, was carried out in the oxidized part of the film, and show that this oxidized spot possess similar characteristics of completely oxidized films, revealing an oxidation propagation mechanism.

Results may be summarized by stating that great modifications were found on the changing from aluminum to aluminum oxide, as suggested by the XRD data, along with the UV–vis transmittance results, which show oxidation increase when the temperature of TA was 550 °C, leading to a transmittance above 60%. A high surface resistivity and lattice vibration related to alumina modes where also found by Raman and FTIR spectra, and are in good agreement with the expected oxidation.

4. Conclusion

The reported results show the influence of temperature, time and atmospheric O_2-concentration of thermal annealing (TA) procedure on the oxidation of aluminum thin films. Temperature about 550 °C is needed in order to modify the Al structure to alumina. TA carried out under room atmosphere conditions show fair oxidation only for TA time above 16 h, whereas TA under O_2-rich conditions show oxidation in much less time, 2 h, which demonstrates the relevance of oxygen gradient, suggesting that the oxygen atomic diffusion or the surface reactivity are determinant processes.

The oxidation was noted through XRD alumina pattern, indicating increase in the alumina peaks intensity, unlike the Al peaks which tend to disappear as the oxidation is accomplished, which leads to increase in the UV–vis transmittance as well. The surface resistivity of oxidized films reaches about 6 orders of magnitude higher compared to as-deposited Al films. FTIR and Raman show the presence of α-Al_2O_3 as well as γ-Al_2O_3, the former one the metastable phase of alumina, in good agreement with XRD findings.

We believe that the investigation presented here is a contribution towards the use of this sort of material as gate in transparent field effect transistor (FET).

Acknowledgments

The authors would like to thank Prof. A. Tabata, for the Raman data, Prof. C. R. Grandini for O_2-rich treatments, and the financial support of the Brazilian agencies: CNPq, FAPESP and FUNDUNESP (Grant 91312/13-DFP).

References

[1] Y. Xuan, H.C. Lin, P.D. Ye, G.D. Wilk, Capacitance–voltage studies on enhancement-mode InGaAs metal-oxide-semiconductor field-effect transistor using atomic-layer-deposited Al_2O_3 gate dielectric, Applied Physics Letters 88 (2006) 263518.
[2] A.I. Kingon, J. Maria, S.K. Streiffer, Alternative dielectrics to silicon dioxide for memory and logic devices, Nature 406 (2000) 1032–1038.
[3] S. Kim, J. Nah, I. Jo, D. Shahrjerdi, L. Colombo, Z. Yao, E. Tutuc, S.K. Banerjee, Realization of a high mobility dual-gated graphene field-effect transistor with Al_2O_3 dielectric, Applied Physics Letters 94 (2009) 062107.
[4] J.C. Chiang, J.G. Hwu, Low temperature (< 400 °C) Al_2O_3 ultrathin gate dielectrics prepared by shadow evaporation of aluminum followed by nitric acid oxidation, Applied Physics Letters 90 (2007) 102902.
[5] C.C. Lin, J.G. Hwu, Nitric acid compensated aluminum oxide dielectrics with improved negative bias reliability and positive bias temperature response, Journal of Applied Physics 113 (2013) 054103.
[6] H.J. Ha, S.W. Jeong, T.Y. Oh, M. Kim, K. Choi, J.H. Park, B.K. Ju, Flexible low-voltage pentacene memory thin-film transistors with combustion-processable Al_2O_3 gate dielectric and Au nanoparticles, Journal of Physics D: Applied Physics 46 (2013) 235102.
[7] C.H. Woo, C.H. Ahn, Y.H. Kwon, J.H. Han, H.K. Cho, Transparent and flexible oxide thin-film-transistors using an aluminum oxide gate insulator grown at low temperature by atomic layer deposition, Metals and Materials International 18 (2012) 1055–1060.
[8] H.C. Lin, P.D. Ye, G.D. Wilk, Current-transport properties of atomic-layer-deposited ultrathin Al_2O_3 on GaAs, Solid-State Electronics 50 (2006) 1012–1015.
[9] J.L.B. Maciel Jr, E.A. Floriano, L.V.A. Scalvi, L.P. Ravaro, Growth of Al_2O_3 thin film by oxidation of resistively evaporated Al on top of SnO_2, and electrical properties of the heterojunction SnO_2/Al_2O_3, Journal of Materials Science 46 (2011) 6627–6632.

[10] L.P.H. Jeurgens, W.G. Sloof, F.D. Tichelaar, E.J. Mittemeijer, Structure and morphology of aluminium-oxide films formed by thermal oxidation of aluminum, Thin Solid Films 418 (2002) 89–101.
[11] S. Kitaoka, T. Matsudaira, M. Wada, Mass-transfer mechanism of alumina ceramics under oxygen potential gradients at high temperatures, Materials Transactions 50 (2009) 1023–1031.
[12] D.R. Askeland, P.P. Phulé, The Sciene and Engineering of Materials, 4th edition, Thomson Learning Inc., Pacific Grove, 2003.
[13] D.L. Smith, Thin Film Deposition – Principles and Practice, 2nd ed., McGraw-Hill, New York, 1995.
[14] L. Ramond, G. Bernard-Granger, A. Addad, C. Guizard, Sintering of soda-lime microspheres using spark plasma sintering, Journal of the American Ceramic Society 94 (2011) 2926–2932.
[15] O. Nast, S. Brehme, S. Pritchard, A.G. Aberle, S.R. Wenham, Aluminum-induced crystallization of silicon on glass for thin-film solar cells, Solar Energy Materials and Solar Cells 65 (2001) 385–392.
[16] S. Gall, M. Muske, I. Sieber, O. Nast, W. Fuhs, Aluminium-induced crystallization of amorphous silicon, Journal of Non-Crystalline Solids 299–302 (2002) 741–745.
[17] G.J. Qi, S. Zhang, T.T. Tang, J.F. Li, X.W. Sun, X.T. Zeng, Experimental study of aluminum-induced crystallization of amorphous silicon thin films, Surface and Coatings Technology 198 (2005) 300–303.
[18] Y. Huang, F. Law, P.I. Widenborg, A.G. Aberle, Crystalline silicon growth in the aluminium-induced glass texturing process, Journal of Crystal Growth 361 (2012) 121–128.
[19] T. Wang, H. Yan, M. Zhang, X. Song, Q. Pan, T. He, Z. Hu, H. Jia, Y. Mai, Polycrystalline silicon thin films by aluminum induced crystallization of amorphous silicon, Applied Surface Science 264 (2013) 11–16.
[20] B.D. Cullity, R. Stock, Elements of X-ray Diffraction, 3rd ed., Prentice Hall, New Jersey, 2001.
[21] S.A. Hassanzadeh-Tabrizi, E. Taheri-Nassaj, H. Sarpoolaky, Synthesis of an alumina – YAG nanopowder via sol–gel method, Journal of Alloys and Compounds 456 (2008) 282–285.
[22] H. Yang, M. Liu, J. Ouyang, Novel synthesis and characterization of nanosized γ-Al_2O_3 from Kaolin, Applied Clay Science 47 (2010) 438–443.
[23] C.L. Lu, J.G. Lv, L. Xu, X.F. Guo, W.H. Hou, Y. Hu, H. Huang, Crystalline nanotubes of γ-AlOOH and γ-Al_2O_3: hydrothermal synthesis, formation mechanism and catalytic performance, Nanotechnology 20 (2009) 215604.
[24] P. Padmaja, K.G.K. Warrier, M. Padmanabhan, W. Wunderlich, F.J. Berry, M. Mortimer, N.J. Creamer, Structural aspects and porosity features of nano-size high surface area alumina–silica mixed oxide catalyst generated through hybrid sol–gel route, Materials Chemistry and Physics 95 (2006) 56–61.
[25] R. Katamreddy, R. Inman, G. Jursich, A. Soulet, C. Takoudis, ALD and characterization of aluminum oxide deposited on Si(100) using Tris (diethylamino) aluminum and water vapor, Journal of the Electrochemical Society 153 (2006) C701–C706.
[26] P.V. Thomas, V. Ramakrishnan, V.K. Vaidyan, Oxidation studies of aluminum thin films by Raman spectroscopy, Thin Solid Films 170 (1989) 35–40.
[27] G.J. Yang, C.X. Li, C.J. Li, Characterization of nonmelted particles and molten splats in plasma-sprayed Al_2O_3 coatings by a combination of scanning electron microscopy, X-ray diffraction analysis, and confocal raman analysis, Journal of Thermal Spray Technology 22 (2013) 131–137.
[28] S. Cava, S.M. Tebcherani, I.A. Souza, S.A. Pianaro, C.A. Paskocimas, E. Longo, J.A. Varela, Structural characterization of phase transition of Al_2O_3 nanopowders obtained by polymeric precursor method, Materials Chemistry and Physics 103 (2007) 394–399.
[29] P.G. Li, M. Lei, W.H. Tang, Raman and photoluminescence properties of a-Al_2O_3 microcones with hierarchical and repetitive superstructure, Materials Letters 64 (2010) 161–163.
[30] W. Wang, J. Huang, Y. Lu, Y. Yang, W. Song, R. Tan, S. Dai, J. Zhou, In situ micro-Raman spectroscopic study of laser-induced crystallization of amorphous silicon thin films on aluminum-doped zinc oxide substrate, Journal of Materials Science: Materials in Electronics 23 (2012) 1300–1305.